Proteomic identification of putative microRNA394 target genes in Arabidopsis thaliana identifies major latex protein family members critical for normal development

Litholdo, Celso G; Parker, Benjamin; Eamens, Andrew L; Larsen, Martin Røssel; Cordwell, Stuart; Waterhouse, Peter M

Published in:
Molecular and Cellular Proteomics

DOI:
10.1074/mcp.M115.053124

Publication date:
2016

Document version
Publisher's PDF, also known as Version of record

Citation for pulished version (APA):
Litholdo, C. G., Parker, B., Eamens, A. L., Larsen, M. R., Cordwell, S., & Waterhouse, P. M. (2016). Proteomic identification of putative microRNA394 target genes in Arabidopsis thaliana identifies major latex protein family members critical for normal development. Molecular and Cellular Proteomics, 15(6), 2033-2047. DOI: 10.1074/mcp.M115.053124

Research

Proteomic Identification of Putative MicroRNA394 Target Genes in *Arabidopsis thaliana* Identifies Major Latex Protein Family Members Critical for Normal Development*[S]

Celso G. Litholdo Jr.‡§ §§, Benjamin L. Parker¶, Andrew L. Eamens‖, Martin R. Larsen, Stuart J. Cordwell¶, and Peter M. Waterhouse‡ ‡‡**

Expression of the F-Box protein Leaf Curling Responsiveness (LCR) is regulated by microRNA, miR394, and alterations to this interplay in *Arabidopsis thaliana* produce defects in leaf polarity and shoot apical meristem organization. Although the miR394-*LCR* node has been documented in Arabidopsis, the identification of proteins targeted by LCR F-box itself has proven problematic. Here, a proteomic analysis of shoot apices from plants with altered *LCR* levels identified a member of the Latex Protein (MLP) family gene as a potential LCR F-box target. Bioinformatic and molecular analyses also suggested that other MLP family members are likely to be targets for this post-translational regulation. Direct interaction between LCR F-Box and MLP423 was validated. Additional MLP members had reduction in protein accumulation, in varying degrees, mediated by LCR F-Box. Transgenic Arabidopsis lines, in which *MLP28* expression was reduced through an artificial miRNA technology, displayed severe developmental defects, including changes in leaf patterning and morphology, shoot apex defects, and eventual premature death. These phenotypic characteristics resemble those of Arabidopsis plants modified to over-express *LCR*. Taken together, the results demonstrate that MLPs are driven to degradation by LCR, and indicate that *MLP* gene family is target of miR394-LCR regulatory node, representing potential targets for directly post-translational regulation mediated by LCR F-Box. In addition, MLP28 family member is associated with the LCR regulation that is critical for normal Arabidopsis development. ***Molecular & Cellular Proteomics 15: 10.1074/mcp.M115.053124, 2033–2047, 2016.***

In eukaryotes, ubiquitination is a post-translational regulatory process that controls the level and/or activity of numerous proteins. Proteins destined for degradation via ubiquitination are covalently conjugated with ubiquitin, a small globular protein that serves as a tag for proteolysis in the 26S proteasome (1–3). Ubiquitination is essential for rapid physiological responses to both internal molecular and external environmental signals, in order for a specific cell or tissue to quantitatively and qualitatively modulate the pool of proteins that make up the proteome at any given time. In the model plant *Arabidopsis thaliana* (Arabidopsis), almost 6% of its known proteome, corresponding to the gene products encoded by 1600 Arabidopsis loci, is predicted to be involved in the ubiquitination-proteasome system (4). It is the multisubunit E3 ubiquitin ligase that directs the specificity of ubiquitination, and in Arabidopsis ~700 genes are predicted to encode the F-box subunit, revealing the biological significance of this component of the ubiquitin pathway for post-translational gene expression regulation in Arabidopsis (5, 6).

F-box proteins are central components of a variety of protein complexes. The Suppressor of Kinetochore Protein 1 (SKP1)-Cullin (CUL)-F-Box (SCF)[1] complexes are the largest

From the ‡School of Biological Sciences, The University of Sydney, Camperdown NSW 2006, Australia; §Laboratório de Biologia Molecular de Plantas, Universidade Federal do Rio de Janeiro, Cidade Universitária, RJ, Brazil; ¶Charles Perkins Centre, School of Molecular Bioscience, The University of Sydney, Darlington NSW 2006, Australia; ‖School of Environmental and Life Sciences, The University of Newcastle, Callaghan NSW 2308, Australia; **Department of Biochemistry and Molecular Biology, University of Southern Denmark, Odense 5230, Denmark; ‡‡Centre for Tropical Crops and Biocommodities, Queensland University of Technology, Brisbane QLD 4001, Australia

Received June 30, 2015, and in revised form, January 27, 2016
Published, MCP Papers in Press, April 11, 2016, DOI 10.1074/mcp.M115.053124

Authors' contributions: CGLJ, ALE and PMW conceived and designed research. CGLJ performed most of the experiments, and BLP performed mass spectrometry and bioinformatics. MRL, SJC, and PMW contributed new reagents or analytic tools. CGLJ, BLP, ALE, MRL, SJC and PMW analysed the data. CGLJ, BLP, ALE, and PMW wrote the manuscript. All authors read and approved the final manuscript.

[1] The abbreviations used are: SCF, Suppressor of Kinetochore Protein1 (SKP1)-Cullin (CUL)-*F*-Box; amiRNAs, artificial miRNAs; ASK, Arabidopsis Skp1-Like; CLV3, Clavata3; C-terminal, Carboxy-terminal; HA, Haemaglutinin; iTRAQ, Isobaric Tags for Relative and Absolute Quantification; LC-MS/MS, Liquid Chromatography Coupled to Tandem Mass Spectrometry; LCR, Leaf Curling Responsiveness; LCR-OE, LCR overexpression plants; LCR-KD, LCR knockdown plants; MLP, Major Latex Protein; N-terminal, Amino-terminal; pro, Promoter; SAM, Shoot Apical Meristem; SOUL, SOUL-Heme-Binding Like Protein; TIR1, Transport Inhibitor Response1; WUS, Wuschel; YFP, Yellow Fluorescent Protein.

and best-characterized group of multisubunit RING domain E3 ubiquitin ligases (7, 8). The F-box is bound to SKP1 via its highly conserved amino (N)-terminal 'F-box' motif, and to its target protein(s) or substrate(s) via its carboxyl (C)-terminal domains (9). The C-terminal region of each F-box protein consists of multiple domains, including WD40 domains, leucine-rich repeats (LRRs), and Kelch repeats (5) in an array of combinations, and it is the C-terminal structural variability that confers F-box target specificity.

In plants, the characterization of a small number of F-box proteins has revealed that they play functional roles in diverse cellular processes, including regulating responses to hormones and mediating pathogen defense as well as directing other essential physiological and developmental processes, including circadian rhythm and flowering time (10, 11). The importance of F-box proteins to plant growth and development is further evidenced by the expression of several F-box-encoding genes under additional post-transcriptional regulation by a class of small regulatory nonprotein-coding RNAs, termed microRNAs (miRNAs). A number of molecular approaches have shown that the expression levels of F-box protein encoding genes, *Transport Inhibitor Response 1* (*TIR1*), *Leaf Curling Responsiveness* (*LCR*) and *More Axillary Growth 2* (*MAX2*) are regulated via miR393-, miR394-, and miR528-directed mRNA-cleavage, respectively (12–14).

In Arabidopsis, miR394 is processed from two precursor transcripts, *PRI-MIR394A* and *PRI-MIR394B* (15). It has been shown to be involved in vasculature and leaf patterning formation (13), and crucial for shoot apical meristem (SAM) stem cell maintenance and competence, by post-transcriptional repression of its F-box target gene *LCR* (16), and more recently demonstrated to be involved in abiotic stress responses (17). The miR394-directed spatiotemporal regulation of *LCR* is crucial for normal SAM development as the inhibition of miR394 activity in the SAM has severe developmental consequences, including downward leaf curvature and eventual meristem termination (13). Although the miR394-LCR node has been well documented in Arabidopsis, the identification of proteins targeted by LCR F-box itself has proven problematic. It has previously been shown that LCR interacts with the well-known SAM stem cell feedback regulators Wuschel (WUS) and Clavata 3 (CLV3); however, neither WUS nor CLV3 is believed to be a direct target of LCR F-box (16).

Here, we used a liquid chromatography coupled to tandem mass spectrometry (LC-MS/MS)-based approach to assess the proteome landscape of the SAM tissue of Arabidopsis plant lines that had been modified to have either elevated (LCR over-expression plants, LCR-OE) or reduced (LCR knockdown plants, LCR-KD) *LCR* levels. This quantitative MS approach identified a number of differentially accumulating proteins, including Major Latex Protein 28 (MLP28), in the modified plant lines. *In silico*, functional and molecular approaches suggested MLP28 as a LCR F-box target and identified other members of the *MLP* gene family as putative targets of LCR-mediated post-translational gene expression regulation. Transgenic plants were produced that expressed artificial miRNAs (amiRNAs) targeted against *MLP28*. These amiRNA-MLP28 lines had diminished *MLP28* levels and displayed severe developmental defects, including elongated petioles, leaf morphology and shoot apex alterations, dwarfness and eventual premature death. These phenotypes resemble those of Arabidopsis plants modified to over-express *LCR*. Taken altogether, the data presented here show that the F-Box LCR mediates the degradation of MLP proteins and that the miR394-LCR node is associated with MLP28, to play a role for normal Arabidopsis development.

EXPERIMENTAL PROCEDURES

Plant material and growth conditions—*Arabidopsis thaliana* (Arabidopsis) ecotype Columbia-0 (Col-0) was used the wild-type (WT) background. Identification of Arabidopsis T-DNA insertion mutant lines was carried out using the Arabidopsis gene mapping tool T-DNA express (http://signal.salk.edu/cgi-bin/tdnaexpress) (18). Transformant lines were generated by floral dipping (19) using *Agrobacterium tumefaciens* (Agrobacterium, strain GV3101)-mediated transformation. Seeds were placed on selective Murashige and Skoog (MS) media that contained the appropriate selective agent to identify primary transformants (T0). T1 lines that segregated at a ratio of ~3:1 on selective plates were transferred to soil for seed collection. Homozygous T2 lines were identified on selective agar plates and confirmed homozygous via standard PCR-based genotyping and used for further phenotypic and molecular analyses. For all Arabidopsis lines used in this study, seeds were stratified via a 48-hour incubation at 4 °C and were subsequently cultivated at 21–23 °C under a 16-hour light/8-hour dark day-night cycle.

Transient Agro-infiltration—Agrobacterium infiltration (Agro-infiltration) method was conducted according to previously described (20). Transient expression assays were performed with 4-week-old wild-type *Nicotiana benthamiana* plants that were cultivated under standard glasshouse conditions of at 22–23 °C and 16-hours of light and 8-hours of dark. Equal volumes of Agrobacterium cultures, each containing the desired binary plasmid, were mixed prior to co-infiltration. Final dilution of cultures used in co-infiltration assays was 0.33OD, and each Agro-infiltration experiment was performed three times and infiltrated leaves were assessed after 3 days of transient expression.

Plasmid constructs—MiR394 overexpression constructs were generated by amplification of 200bp of the precursor of *MIR394B*, flanking mature miRNA sequences, and fused to *Cauliflower mosaic virus* (CaMV) 35S promoter (35Spro) presented in the pART7 vector (21). Subsequent cloning steps were performed by excision of the 35Spro/miRNA overexpression sequence/terminator fragment using NotI restriction digestion, ligation into similarly digested vector pART27, and generation of plant expression vector (21). MiR394 sponge constructs were generated by GeneArt Gene Synthesis (Life Technologies, Carlsbad, CA/USA). The STTM format followed the design of Yan *et al.* (2012), and construct designs are illustrated in supplemental Fig. S1. Nucleotide sequences were designed to target miR394, and contained additional spacer nucleotides and 5′ XhoI and 3′ XbaI restriction sites, for subsequent cloning steps in pART7 and pBART, generating plant expression vector (22). MiRNA-resistant *LCR* transgene (LCR-OE) was generated by site-directed mutagenesis using the QuikChange Lightning Multisite-Directed Mutagenesis Kit according to the manufacturer's instructions (Agilent Technologies, Santa Clara, CA/USA). The modified sequence was subsequently cloned into the plant expression vector pBART.

Gateway-compatible plant transformation pEarleyGate201, obtained from TAIR was used to epitope tag (HA; hemagglutinin) the N terminus of each protein of interest (23). Amplicons of the *LCR* and *TIR1* coding sequences were fused in frame to the *Cauliflower mosaic virus* 35S promoter (35Spro) housed in the shuttle vector pART7. The resulting 35S promoter/gene of interest fragments were subsequently cloned into the plant expression vector pBART. The pBART vector alone (no inserted sequences) used as the empty vector control and the *GUS* plant expression vector (35Spro::GUS; pBART housing a 35S promoter-GUS fragment) was used as Agrobacterium infiltration internal control.

Gateway-compatible plant transformation pSITE-YFP vectors, obtained from TAIR, were used to express fusions to monomeric YFP for the expression in plant cells (24, 25). The N-terminal region of YFP was fused with MLP28 and MLP423 and the YFP C terminus was next fused with LCR F-box. Bimolecular fluorescence complementation (BiFC) were performed as previously described (26). Plants agro-infiltrated for the BiFC assay were assessed for YFP expression under the stereo fluorescence microscope with FITC and YFP filter sets (SteREO Lumar V12, SteREO Lumar V12, Zeiss, Oberkochen, Germany).

β-Glucuronidase (*GUS*) reporter gene constructs were generated by PCR amplification of genomic fragments, immediately upstream of the start codons of *MIR394A* (4 Kb), *MIR394B* (4 Kb), *LCR* (1.6 Kb, plus additional 1.1 Kb downstream of ATG sequence), *MLP28* (1.6 Kb) and *MLP423* (1.8 Kb), which were subsequently cloned into the pRITA::GUS vector (21). Subsequently, the generated promoter::GUS fragment was cloned into the plant expression vector pBART. Staining for GUS activity determination was performed as previously described (27). Images of GUS stained plants were obtained using the stereo fluorescence microscope under white light.

Artificial miRNAs were generated to direct RNA silencing of *MLP28* using the pBlueGreen vector system that includes the *MIR159B* primary miRNA coding sequence fused to the 35S promoter (28).

All generated plant expression vectors were used to stably transform wild-type Arabidopsis plants via Agrobacterium-mediated transformation. All oligonucleotides used in this study to generate plant expression vectors via a PCR-based cloning approach are all listed in supplemental Table S1.

Mass spectrometry analysis—Proteins were extracted from shoot apices dissected from *Arabidopsis* seedlings [~8 plants per biological replicate; wild-type *Arabidopsis* and LCR-overexpression (OE) and LCR-kockdown (KD) transformant lines] as described previously (29). Briefly, apices were tip-probe sonicated (3 × 30 s) in 8 M urea, 1% triton X-100 in 100 mM triethylammonium bicarbonate (TEAB) (pH 7.5) and centrifuged at 13,000 × *g* for 10 min. The supernatant was precipitated with 20% trichloroacetic acid overnight at −20 °C and the protein pellets washed briefly with ice-cold acetone. Proteins were resuspended in 8 M urea in 100 mM TEAB (pH7.5), reduced with 10 mM dithiothreitol for 60 min at room temperature and alkylated with 25 mM iodoacetamide for 60 min at room temperature in the dark. The reaction was diluted 5-fold with 100 mM TEAB and digested with trypsin (1:50 trypsin/protein) overnight at 37 °C. Peptide preparation, stable isotope labeling with isobaric tags for relative and absolute quantitation (iTRAQ; AB Sciex, Framingham, MA), peptide fractionation, and nano-reverse phase liquid chromatography- electrospray ionization- tandem mass spectrometry (LC-MS/MS) was performed as described previously (30). Briefly, 100 μg of peptide was labeled with iTRAQ according to the manufacturer's instructions and desalted with hydrophilic-lipophilic balance solid phase extraction (Waters; Milford, MA). The peptides were resuspended in 90% acetonitrile, 0.1% TFA and fractionated into 10–11 fractions on an in-house packed amide-HILIC column (320 μm x 17 cm with μm particles; Tosho, Tokyo, Japan) using an Agilent 1200. The gradient was 90–60% acetonitrile containing 0.1% TFA over 30 min at 6 μl/min. Each fraction was resuspended in 0.1% formic acid and separated on an in-house packed C18AQ column (75 μm x 17 cm with 3 μm particles; Dr Maisch, Ammerbuch,Germany) using an Easy nLC-II. The gradient was 0–30% acetonitrile containing 0.1% formic acid over 120 min at 250 nl/min. The separation was coupled to either an LTQ-Orbitrap XL or LTQ-Orbitrap velos. For LTQ-Orbitrap XL analysis, an MS1 precursor scan was measured at 400–1600 *m/z* (30,000 resolution and $1e^6$ AGC) followed by data-dependent MS2 analysis by both LTQ-CID (35 NCE and $3e^4$ AGC) and Orbitrap-HCD (55 NCE, 7500 resolution and $4e^5$ AGC) of the top three most intense ions. For LTQ-Orbitrap velos analysis, a similar data-dependent acquisition was performed except the top seven most intense ions were analyzed by Orbitrap-HCD only (48 NCE, 7,500 resolution and $4e^4$ AGC). An additional biological replicate was performed with 3-plex dimethyl labeling essentially as described previously (31). These peptides were fractionated by amide-HILIC and analyzed on an LTQ-Orbitrap XL essentially as described above excepted data-dependent acquisition was performed on the top ten most intense ions with LTQ-CID. All resulting raw data were processed using Proteome Discoverer v1.4beta (Thermo Fisher Scientific, Waltham, MA/USA) and searched against the *Arabidopsis* TAIR-10 database (35,386 entries) with SequestHT. The parameters included a tolerance of 20 ppm for MS1 and 0.02 Da for HCD-MS/MS or 0.6 Da for CID-MS/MS. The data was searched with Met oxidation as a variable modification and Cys carbamidomethylation as a fixed modification with either fixed modification of iTRAQ peptide N terminus and Lys or, fixed modification of 3-plex demethylation of peptide N terminus and Lys (in three separate searches). The enzyme was full trypsin cleavage and all results were filtered to 1% FDR with Percolator (32). Proteins were normalized to the median of all peptide spectral matches and statistical analysis was conducted in Perseus. The mass spectrometry proteomics data have been deposited to the ProteomeXchange Consortium (33) with the data set identifier PXD002390.

Experimental Design and Statistical Rationale—For the proteomic analysis of plant tissue, a total of three biological replicates were performed where each replicate consisted of eight pooled dissected shoot apices from Arabidopsis transformant seedlings. We investigated differentially regulated proteins between both over-expression and knockdown of LCR relative to wild-type. We hypothesized that protein(s) regulated by LCR would show both decreased expression with LCR overexpression and increased expression with LCR knockdown and, these proteins would be prioritized for further validation. Because of available starting material and resources, two biological replicates were performed with iTRAQ and one additional biological replicate was performed with 3-plex dimethylation. Identification of significantly regulated proteins was performed by analyzing the two iTRAQ replicates with a one-sample *t* test corrected for multiple testing with a Benjamini Hochberg FDR of 1%. Significantly regulated proteins were further filtered to display only very high confident hits to validate which displayed >50% fold-change in both biological replicates and displayed >50% regulation in the third dimethylation biological replicate. Although we hypothesized LCR-dependent regulation would result in differential abundance between overexpression and knockdown and this would enable efficient stratification of targets for validation, the observed reciprocal response was not robust and there were very little proteome changes. There are numerous reasons why this reciprocal regulation was not observed. For example, overexpression of an E3 ligase may not necessarily result in robust down-regulation of target proteins because other cofactors or the proteasome itself may be rate-limiting. However, because the candidate list of proteins was small, we attempted validation for a number of targets.

Western Blot Analysis—Proteins were extracted in extraction buffer [100 mM Tris HCl pH 8.0, 0.04% DTT, 10% glycerol, and protease

TABLE I
LCR-like proteins identified in a variety of plant species contain a putative F-Box motif region

LCR-like protein (accession #)	Plant species	Family	Size (aa)	F-Box motif (aa region)
NP_564278	*Arabidopsis thaliana*	Brassicaceae	467	112–158
XP_002890723	*Arabidopsis lyrata*	Brassicaceae	463	108–154
ACL51019	*Citrus trifoliata*	Rutaceae	468	114–160
XP_003538543	*Glycine max*	Fabaceae	450	96–142
ACI13687	*Malus domestica*	Rosaceae	472	118–164
Nbv3K765635121[a]	*Nicotiana benthamiana*	Solanaceae	458	107–153
XP_002297845	*Populus trichocarpa*	Salicaceae	481	127–173
XP_004239218	*Solanum lycopersicum*	Solanaceae	466	112–158
XP_002271194	*Vitis vinifera*	Vitaceae	522	168–214
NP_001045243	*Oryza sativa*	Poaceae	443	89–135
AFW84117	*Zea mays*	Poaceae	443	89–135

[a] Sequence retrieved from the *Nicotiana benthamiana* genome webpage (http://benth-web-pro-1.ucc.usyd.edu.au/blast/blast.php).

inhibitor tablet cOmplete ULTRA Tablets (Roche, Basel, Switzerland)] and concentration was determined using the Protein Assay kit (Bio-Rad, Hercules, CA/USA). SDS-PAGE polyacrylamide midi gels NuPAGE Bis-Tris (Life Technologies) were used to separate 10 μg of total protein under denaturing conditions. Western blotting was conducted by probing electroblotted nitrocellulose membranes with monoclonal anti-HA antibody (1:10,000; Sigma-Aldrich, St. Louis, MO/USA) or anti-β-glucuronidase (N-Terminal) antibody (1:5000; Sigma-Aldrich) and a shared host-specific secondary antibody. Bands were visualized with the Western Lightning Plus ECL (Perkin-Elmer, Waltham, MA/USA). Assays were repeated at least 3 times per each analyzed MLP-HA tagged protein.

Quantitative RT-PCR (RT-qPCR) Analysis—Total RNA was extracted from frozen plant material using TRIzol Reagent according to the manufacturer's instructions (Life Technologies). For RT-qPCR, 5 μg of DNase (Promega, Fitchburg, WI/USA)-treated total RNA was used for first-strand cDNA synthesis with oligo $(dT)_{23}$ primer and reverse transcription with the Superscript III reverse transcriptase (Life Technologies) according to the manufacturer's protocol. RT-qPCR was carried out on an Mx3000P instrument (Agilent Technologies), and Brilliant II SYBR Green QPCR Master Mix (Agilent Technologies) was used for the three-step cycling reactions, following the manufacturer's instructions. All RT-qPCR reactions (for both reference and specific genes) were carried out in biological and technical triplicate. *Cyclophilin* (*Cyclophilin 5*; *AT2G29960*) was used to normalize gene expression using the comparative quantification program and data was analyzed with MxPro QPCR Software (Agilent Technologies).

Protein Identification, Alignment and Structure Predictions—Searches of available plant proteome was carried out using the NCBI pairwise Basic local alignment search tool (BLASTp) (http://blast.ncbi.nlm.nih.gov/Blast.cgi) (34). Multiple sequence alignment and phylogram tree were obtained by the program Geneious (http://www.geneious.com/). Identification of LCR motifs was carried out using the software PFAM (http://pfam.sanger.ac.uk/) (35), and REP (http://www.bork.embl.de/~andrade/papers/rep/search.html) (36). LCR protein secondary and tertiary structures were predicted with the software Protein Homology/analogy Recognition Engine V2.0 (PHYRE2) (http://www.sbg.bio.ic.ac.uk/phyre2/html/page.cgi?id=index) (37), and modeling was refined by the Chiron protein minimization server (http://dokhlab.unc.edu/tools/chiron/) (38). LCR-interacting proteins was identified and plotted by the software Search Tool for the Retrieval of Interacting Genes/Proteins (STRING) (http://string-db.org/) (39).

RESULTS

In Silico Analysis of the Structure of LCR F-box-like Proteins—Extensive BLASTP searches of publically available plant proteome data sets (http://blast.ncbi.nlm.nih.gov/Blast.cgi) (34), using the 467-amino acid (aa) sequence of the Arabidopsis LCR F-box as the query, generated an extensive list of putative LCR F-box-like proteins. This initial list was reduced to 11 unique full-length LCR-like proteins (Table I), and each contained an N-terminal F-box motif with similarity to residues 112 to 158, of the Arabidopsis LCR query sequence (Table I and Fig. 1*A*). These F-Box motif sequences showed a high level of conservation even though they come from evolutionary diverse plant species (Fig. 1*A*). Bioinformatic analysis of the secondary structure of the Arabidopsis LCR F-box C terminus revealed that this region contains a number of putative protein-protein interaction domains, termed Kelch repeats. Four Kelch repeats were detected, at LCR aa residues 163–211, 252–305, 307–354, and 406–456 (Fig. 1*A*). In addition, a high level of sequence conservation was also detected in the C-terminal region of the 11 assessed LCR F-box-like proteins, which at nucleotide level contain the miR394 target site also conserved, to further indicate that each is a true representative of a LCR F-box-like protein encoded by each respective plant species (data not shown).

The secondary and tertiary structure of Arabidopsis LCR was predicted and the three-dimensional model shows two distinct structural domains: (1) an F-box motif in the N terminus forming a stem-like structure, and; (2) a C-terminal domain, consisting of four Kelch repeats that make a solenoid-like structure (Fig. 1*B*). Together, the four Kelch repeats form a four-stranded β-sheet, which, via hydrophobic interactions, generate a conserved β-propeller tertiary structure (Fig. 1*C*). In addition to this *in silico* evidence for Arabidopsis LCR to function as a canonical F-box protein, previous protein-protein interaction studies (40) have demonstrated that Arabidopsis LCR interacts with multiple members of the Arabidopsis SKP1-like (ASK) family (Fig. 1*D*).

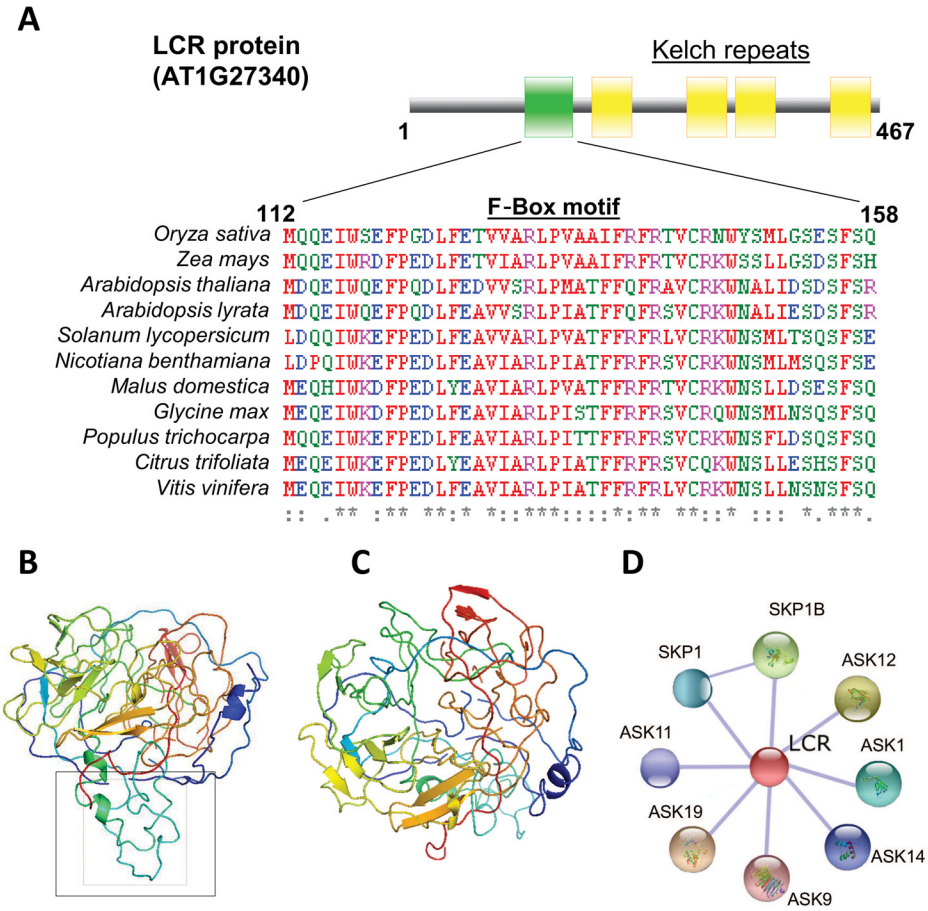

FIG. 1. **In silico analyses of the Arabidopsis LCR F-box.** *A*, Schematic of the functional domains of the Arabidopsis LCR F-box, and amino acid sequence alignment of the predicted LCR F-box motif in 11 diverse plant species, including monocotyledoneous and dicotyledonous representatives. *B*, The three-dimensional structure prediction for the Arabidopsis LCR F-Box. The region corresponding to the N-terminal-localized F-box motif is indicated by the dashed-line box. *C*, The four-stranded β-propeller structure that the Arabidopsis LCR F-box is predicted to adopt because of the four adjacent Kelch repeat domains in the C terminus. *D*, Experimentally validated proteins demonstrated to interact with the Arabidopsis LCR F-box, and all eight of these interacting proteins are members of the *Arabidopsis* SKP-like (ASK) protein family.

Generation of Arabidopsis Plants with Altered MicroRNA394 and LCR Levels—Several approaches were used to generate transgenic plants with altered miR394-LCR regulatory pathway, in which either miR394 or *LCR* levels were directly targeted for deregulation. To specifically alter miR394 accumulation, miR394 overexpressing transgenic plant lines (miR394-OE) were generated by transforming plants with a construct containing 200bp of the precursor *MIR394B*, flanking the mature miR394 sequence. MIR394-OE plant lines highly accumulated miR394 as assessed by small RNA northern blotting and displayed upward leaf curvature when compared with WT plants (Fig. 2*A* and 2*B*). We next attempted to generate miR394A/B knockdown Arabidopsis lines using two different "sponge" approaches (41). This technology uses complementary nucleotide sequences to the mature miRNA including mismatches between bases 10 and 11, preventing slicer activity of AGO proteins, and hence acting as a "sponge" of mature miRNAs sequences. In the first format, the miR394-SPO sponge construct was made from an artificially synthesized DNA sequence encoding 10 non-cleavable repeated regions complementary to miR394 sRNA but harboring mismatched bases across the cleavage site (supplemental Fig. S1*A*). However, using this approach, miR394 levels matched WT lines as assessed by small RNA northern blotting, and the miR394-SPO transformed lines closely resembled WT plants (Fig. 2*A* and 2*B*). The second format followed the design of short tandem target mimic (STTM) constructs (42) (supplemental Fig. S1*B*). Successful knockdown was achieved below the limit of detection as assessed by small RNA northern blotting and the miR394-STTM plant lines displayed a range of altered morphology, including dramatically down-curled leaves (Fig. 2*A* and 2*B*).

To alter *LCR* levels, a miR394-resistant *LCR* construct, with an altered miR394-binding site containing four silent point mutations was transformed into WT plants (supplemental Fig. 2*A*). Referred herein as LCR-OE plants (*LCR* overexpression),

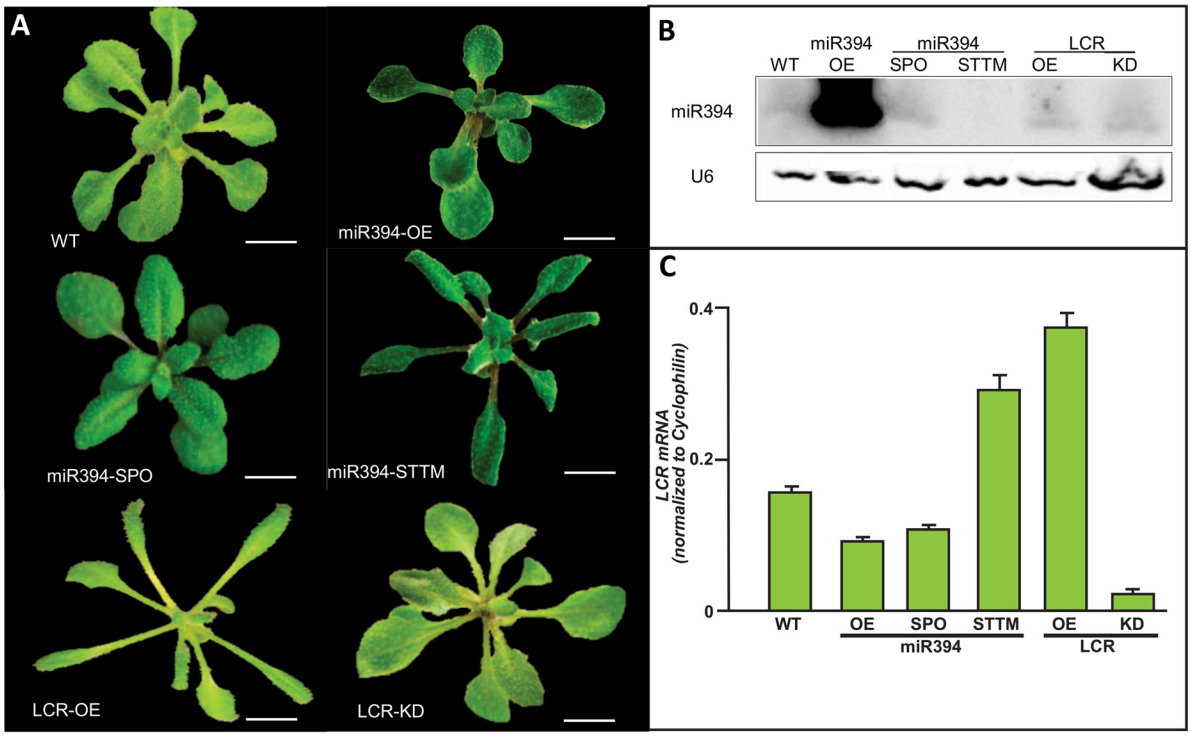

FIG. 2. **MIRNA394- and LCR-deregulated transgenic Arabidopsis lines.** *A*, Phenotypic analyses of Arabidopsis plants with altered miR394-targeted *LCR* gene levels. Wild type (WT); miR394 overexpressing line (miR394-OE); miR394 sponge construct SPO (miR394-SPO); miR394 sponge construct STTM (miR394-STTM); miR394-resistant *LCR* line (LCR-OE); T-DNA insertional mutant (LCR-KD). *B*, Differential mature miR394 accumulation in WT, miR394-OE, miR394-SPO, miR394-STTM, LCR-OE, and LCR-KD plant lines. End-labeled DNA oligonucleotides complementary to the miR394 sRNA and U6 were assessed by sRNA-specific northern blotting. *C*, Comparative quantification of *LCR* gene expression relative to *Cyclophilin* was determined by quantitative RT-qPCR analysis. These data support the description of *LCR* as the target gene of miR394.

these transformants displayed ~2- to 3-fold increase in *LCR* mRNA and a pronounced change in leaf morphology (Fig. 2*A* and 2*C*). Some of the lines showed severe developmental defects, characteristic of shoot apical meristem (SAM) termination, leading to premature death and failure to flower (supplemental Fig. S2*B*–S2*E*). Conversely, Arabidopsis plant lines with greatly reduced *LCR* expression were obtained from the SALK collection of T-DNA insertion mutant lines (18). The T-DNA insertion is in the first exon of the *LCR* gene (SALK_136833). These plants, hereafter named LCR-KD (*LCR* knock down) had 4–5-fold reduced expression of *LCR* mRNA and showed a subtle leaf polarity phenotype with the leaves curling in a slightly upwards direction, similar to that observed in the miR394-OE plants (Fig. 2*A* and 2*C*).

The transgenic plants with altered miR394 expression were also assessed for *LCR* mRNA levels by RT-qPCR (Fig. 2*C*). This demonstrated an inverse relationship between the *LCR* mRNA levels and the observed phenotype. Specifically, overexpression of miR394 reduced *LCR* mRNA levels and resulted in leaves curling in an upwards direction. This phenotype was recapitulated by directly knocking down *LCR*. Alternatively, knocking down miR394 increased *LCR* mRNA levels resulting in leaves curling downwards combined with developmental defects. This phenotype was also recapitulated by directly overexpressing *LCR*.

Identification of Differential Proteins in Arabidopsis Plants with Altered LCR Levels—To identify LCR F-box regulated proteins, proteomic analysis was performed from the shoot apex of WT and the transformant lines, LCR-OE and LCR-KD. LCR-OE and LCR-KD lines were selected as they had been previously determined to have the most elevated and reduced *LCR* expression, respectively, among the transgenic lines (Fig. 2*C*). Proteins from the three groups were digested with trypsin and labeled with isobaric tags for relative and absolute quantification (iTRAQ) in biological duplicate prior to analysis by LC-MS/MS. An additional biological replicate was performed using 3-plex dimethyl labeling and LC-MS/MS which served as validation. A total of 4676 proteins were identified in the iTRAQ replicates with 3093 quantified with ≥2 peptides in both biological replicates (Fig. 3*A* and supplemental Table S2–S3). These data showed very low global variation and only two proteins were up-regulated with LCR-KD and one protein down-regulated with LCR-OE (>1.5-fold and adjusted $p < 0.05$). The single protein down-regulated with LCR-OE was the major latex protein 28 (MLP28; AT1G70830.1) whereas the two proteins up-regulated with LCR-KD were SOUL-like

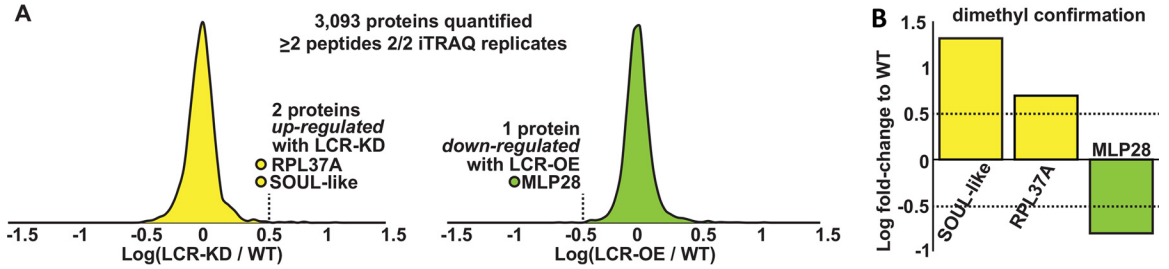

FIG. 3. **Protein groups differentially accumulating in LCR-OE and LCR-KD transformant lines.** *A*, Distribution of 3,093 proteins quantified in biological duplicate and presented as LCR-OE/WT and LCR-KD/WT ratios. Highlighted are three significantly regulated proteins (>50% regulation and adjusted $p < 0.05$; one sample *t* test) *B*, Dimethylation validation of three proteins regulated with either LCR-KD (yellow) or LCR-OE (green).

heme containing protein (AT1G17100.1) and the zinc-binding ribosomal-like protein (RPL37A; AT1G15250.1). Of the 3093 proteins quantified in both iTRAQ replicates, a total of 2922 proteins were quantified in the 3-plex dimethylation experiment. The three proteins regulated in both iTRAQ experiments were similarly regulated in the dimethylation experiment (Fig. 3*B*).

Transient co-expression of LCR and MLP28 results in reduced MLP28 accumulation—To experimentally test whether MLP28 and SOUL are targeted by LCR for post-translational regulation, plasmids (35Spro::MLP28::HA and 35Spro::SOUL::HA) encoding hemaglutinin (HA)-tagged versions of both putative targets were generated. Young leaves of *Nicotiana benthamiana* plants were independently Agro-infiltrated with these constructs and the accumulation of MLP28 and SOUL assessed, by Western blotting. In all experiments, MLP28-HA accumulated to high levels but the levels of SOUL-HA were undetectable; further analysis of SOUL was therefore not pursued.

To verify that MLP28 is a specific target of LCR F-box, the 35Spro::MLP28::HA vector was co-infiltrated into young *N. benthamiana* leaves along with four F-box vectors: (1) 35Spro::LCR, encoding a full-length wild-type version of the Arabidopsis LCR gene; (2) 35Spro::mLCR, encoding a modified miR394-resistant full-length version of the Arabidopsis *LCR* gene (supplemental Fig. S2*A*); (3) LCRpro::mLCR, encoding the modified *LCR* transgene under the control of the endogenous *LCR* promoter, and; (4) 35Spro::P0, which produces the unrelated, but well-characterized, *Polerovirus* P0 F-box protein. Co-infiltration of the 35Spro::MLP28::HA with the P0 or with an "empty" 35Spro::HA construct were measures taken to monitor for nonspecific effects.

Western blotting showed that MLP28-HA expressed from the 35Spro::MLP28::HA construct accumulated to high levels when co-infiltrated with empty vector (Fig. 4*A*). Co-expression of MLP28-HA with *LCR* from either the 35Spro::LCR or 35Spro::mLCR constructs, resulted in a marked reduction in MLP28 levels as assessed by anti-HA Western blotting. A slight reduction in MLP28 levels was observed with co-expression of MLP28-HA with the LCRpro::mLCR construct. This is consistent with LCR targeting MLP28 for ubiquitination and hence degradation. The undiminished MLP28-HA levels from co-infiltration with 35Spro::P0 indicates that the reduction of MLP28-HA accumulation in these experiments was specifically caused by LCR.

Degradation of Additional MLP Gene Family Members by Arabidopsis LCR F-box—The regulation of MLP28 in LCR transgenic Arabidopsis lines identified by quantitative proteomics and, the co-expression analysis in Agro-infiltrated *N. benthamiana* leaves suggested that MLP28 is targeted by the Arabidopsis LCR for post-translational regulation. We therefore performed a bioinformatics analysis of 12 additional members of the highly conserved Arabidopsis *MLP* gene family. Comparison of their amino acid (aa) sequences showed that MLP28 has its highest sequence identity with MLP31, MLP34, and MLP43 (supplemental Fig. S3*A*) and together they form a phylogenetic clade that is distinct from MLP165, MLP168, MLP328, MLP329, and MLP423 (supplemental Fig. S3*B*). The tertiary structures of each of *Arabidopsis MLP* gene family members was predicted (supplemental Fig. S4) and revealed that they all adopt highly similar structures, despite only regions of similar sequences. This suggested that multiple *MLP* gene family members could be potential targets of LCR F-box-mediated post-translational gene expression regulation.

We next investigated the potential regulation of additional MLP family members by LCR. The full-length sequences of four *MLP* gene family members were cloned into a HA-tagged plant gene expression vector. Three of them, *MLP31*, *MLP34,* and *MLP43*, are highly similar to *MLP28* whereas *MLP423*, has less sequence similarity. Each of the four MLP::HA expression vectors was co-infiltrated into young *N. benthamiana* leaves along with either; (1) an empty control vector; (2) the 35Spro::LCR vector, or; (3) the 35Spro::TIR1 vector, which is a well-characterized plant F-box protein and was included as a negative control. Western blotting revealed that co-expression of the 35Spro:LCR vector with each of the four MLP::HA vectors negatively affected the abundance of each HA-tagged MLP (Fig. 4*B*–4*E*). The MLP31 and MLP34 HA-tagged proteins showed dramatically decreased accumulation when co-expressed with the *LCR* transgene, but not when co-infiltrated with the *TIR1* vector (Fig. 4*B* and 4*D*). When co-expressed

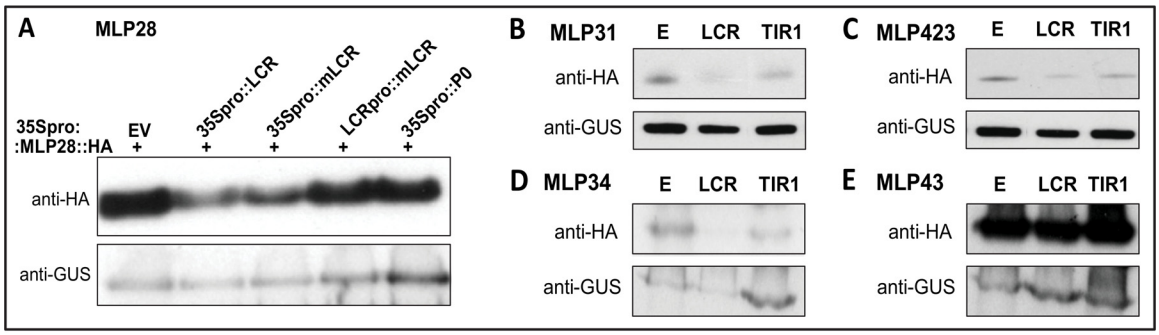

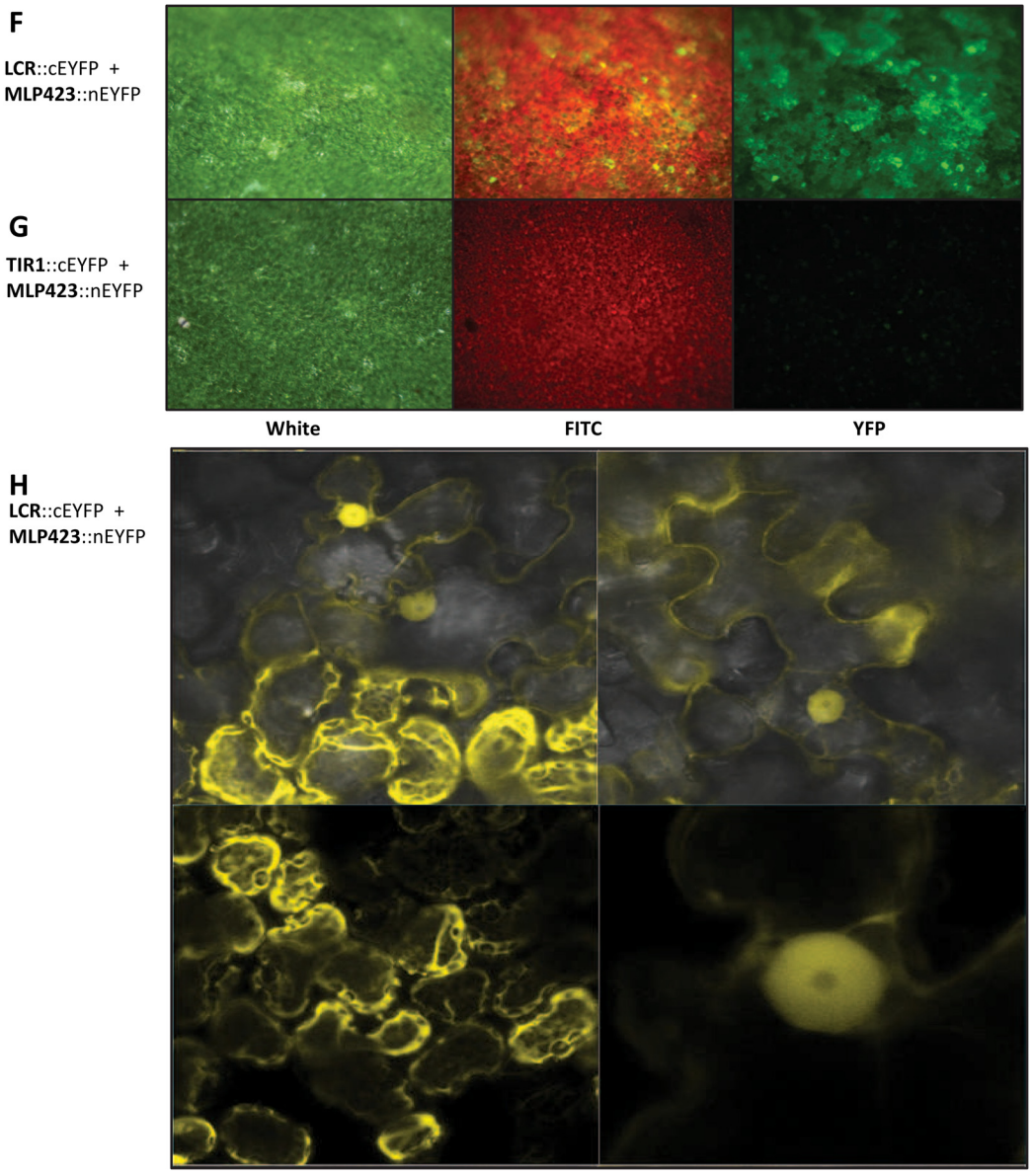

FIG. 4. **Western blotting analysis of epitope-tagged MLPs and positive BiFC assay for LCR and MLP423 physical interaction.** *A*, Western blot analysis of proteins extracts sampled from *N. benthamiana* leaves transiently co-expressing the MLP28:HA vector (top panel) along with; an empty HA-tag vector (lane 1); an unmodified *LCR* transgene (lane 2); a miR394-resistant *LCR* transgene (lane 3); a miR394-resistant *LCR* with endogenous *LCR* promoter (lane 4), and; the viral RNA silencing suppressor protein, the P0 F-box (lane 5). *B*, Western blot analysis of protein extracts sampled from *N. benthamiana* leaves transiently co-expressing unmodified, and HA-tagged versions of additional MLP gene family members MLP31, and *C*, MLP34, along with; an empty HA-tag vector (lane 1); an unmodified *LCR* transgene (lane 2), and;

with *LCR* transgene, a modest reduction in MLP43 and MLP423 HA-tagged protein levels was detected by Western blotting (Fig. 4*C* and 4*E*). Together, these results show that MLP proteins are degraded by LCR and strongly suggested that other *MLP* gene family members in addition to MLP28 are targeted by LCR F-box for post-translational gene expression regulation.

In Vivo Assessment of LCR F-box Target Interaction—The Bimolecular Fluorescence Complementation (BiFC) assay was used to study protein-protein interactions *in vivo* (25). BiFC assay relies on the fluorescent signal that only forms when two fragments of a fluorescent protein is brought together by physical interaction of the proteins under investigation, which is fused to these fragments. In order to determine if the observed degradation of MLP proteins in the presence of LCR F-Box is directly driven by the physical interaction of the targeted MLP with LCR, two *MLP* gene family representatives with lower sequence similarity, namely MLP28 and MLP423, were selected for inclusion in this analysis.

BiFC analysis demonstrated *in vivo* interaction between LCR F-Box and MLP423 via the clear visualization of Yellow Fluorescent Protein (YFP) in *N. benthamiana* leaves co-expressing LCR:cYFP and MLP423:nYFP vectors (Fig. 4*F*). In addition, no fluorescence was observed when the TIR1::cYFP negative control vector was co-infiltrated with MLP423::nYFP vector (Fig. 4*G*). Furthermore, confocal microscopy revealed that LCR F-Box and MLP423 interaction occurred in the nuclear envelope and in the cytoplasm of YFP-expressing cells (Fig. 4H). No YFP fluorescence was observed in *N. benthamiana* leaves co-expressing LCR:cYFP and MLP28:nYFP vectors (data not shown). Together, these results indicate that the detection of physical interaction between LCR and MLP423, and not between LCR and MLP28, may be because of a more rapid degradation rate of MLP28, brought about by LCR F-box-directed ubiquitination, than MLP423.

MLP28 and MLP423 Gene Expression in Arabidopsis—To determine if the expression domains of *MLP28* and *MLP423* overlap with those previously determined for *MIR394A*, *MIR394B,* and *LCR* (supplemental Fig. S6), promoter-GUS expression vectors *MLP28*pro::GUS and *MLP423*pro::GUS were generated.

In *Arabidopsis* plants stably transformed with the *MLP28*pro::GUS, the GUS staining was clearly visible in the vasculature of rosette leaves, petioles, lateral root meristems, anther filaments and developing siliques, as well as in the embryonic tissues of developing seeds (Fig. 5*A*–5*F*). In *MLP423*pro::GUS lines, GUS activity was observed at low levels in all vegetative tissues of young plants, and more intensely in the petioles and at the base of newly emerged and emerging leaves (Fig. 5*G*). In more mature *MLP423*pro::GUS plants, the *GUS* staining was restricted to the base of trichomes, in the leaf (Fig. 5*H*), and to sepals, petals, anther filaments and the style, in floral tissues (Fig. 5*I*). *MLP423* promoter activity was visible throughout mature silique tissues but had a more restricted pattern in developing siliques (Fig. 5J). It was also evident in the seeds of *MLP423*pro::GUS plants (Fig. 5*K*–5*L*).

These observed expression domains partially correlate with those of *MIR394A*, *MIR394B* and *LCR* (supplemental Fig. S5). This shows that *MLP28* and *MLP423*, are transcribed in vegetative and/or reproductive tissues where LCR F-box can regulate the stability of their encoded proteins.

Characterization of Arabidopsis plants with repressed MLP expression—To assess whether disrupted *MLP28* and *MLP423* expression would have a negative effect on Arabidopsis development, putative T-DNA knockout insertion mutant lines were obtained from the publically available collection (18). Homozygous mutant plant lines *mlp28* (CS366498), *mlp423–1* (SALK_042869) and *mlp423–2* (SALK_022306C) were characterized at both the phenotypic and molecular level.

Molecular analyses confirmed down-regulation of the *MLP423* gene in the two lines, with both *mlp423–1* and *mlp423–2* displaying mild alterations in the leaf curvature (supplemental Fig. S6). At the phenotypic level, *mlp28* plants were indistinguishable from WT (Fig. 6*A*). At the molecular level, RT-qPCR showed that *MLP28* expression was highly elevated (Fig. 6E). The T-DNA insertion in *mlp28* is immediately 5′ of the *MLP28* transcription start site which may explain its elevated, rather than repressed, transcription.

The alternative approach of using artificial miRNA (amiRNA) technology (43, 28, 44) was used as an alternative method to knockdown *MLP28* expression. Two lines, termed amiR-MLP28 1.2 and amiR-MLP28 1.3, had reduced *MLP28* expression (Fig. 6*E*). AmiR-MLP28 1.2 plants displayed elongated petioles and alterations in leaf curvature (Fig. 6C) and a 3-fold reduction in *MLP28* (Fig. 6*E*). Plants of the amiR-MLP28 1.3 line had even greater repression of *MLP28* and showed severe developmental abnormalities, including dwarf plants with strong alterations in leaf patterning and morphology, and

an unmodified *TIR1* transgene (lane 3). *D*, Western blot analysis of protein extracts sampled from *N. benthamiana* leaves transiently co-expressing unmodified, and HA-tagged versions of additional MLP gene family members MLP43, and *E*, MLP423 along with; an empty HA-tag vector (lane 1); an unmodified *LCR* transgene (lane 2), and; an unmodified *TIR1* transgene (lane 3). *A–E,* A *GUS* expression vector was used as the Agrobacterium infiltration internal control and western loading control (bottom panels). *F*, BiFC assay demonstrated physical interaction between LCR F-box and MLP gene family member MLP423. *G*, Microscopy of *N. benthamiana* leaves co-expressing the TIR1:cYFP and MLP423:nYFP plant expression vectors. *F–G*, Images were captured under white light (left panel), the fluorescein isothiocyanate filter (FITC; middle panel), and YFP filter (right panel). *H*, Confocal microscopy demonstrated that YFP fluorescence in *N. benthamiana* leaf cells co-expressing LCR::cYFP and MLP423::nYFP transgenes was localized to both the nuclear envelope and the cytoplasm.

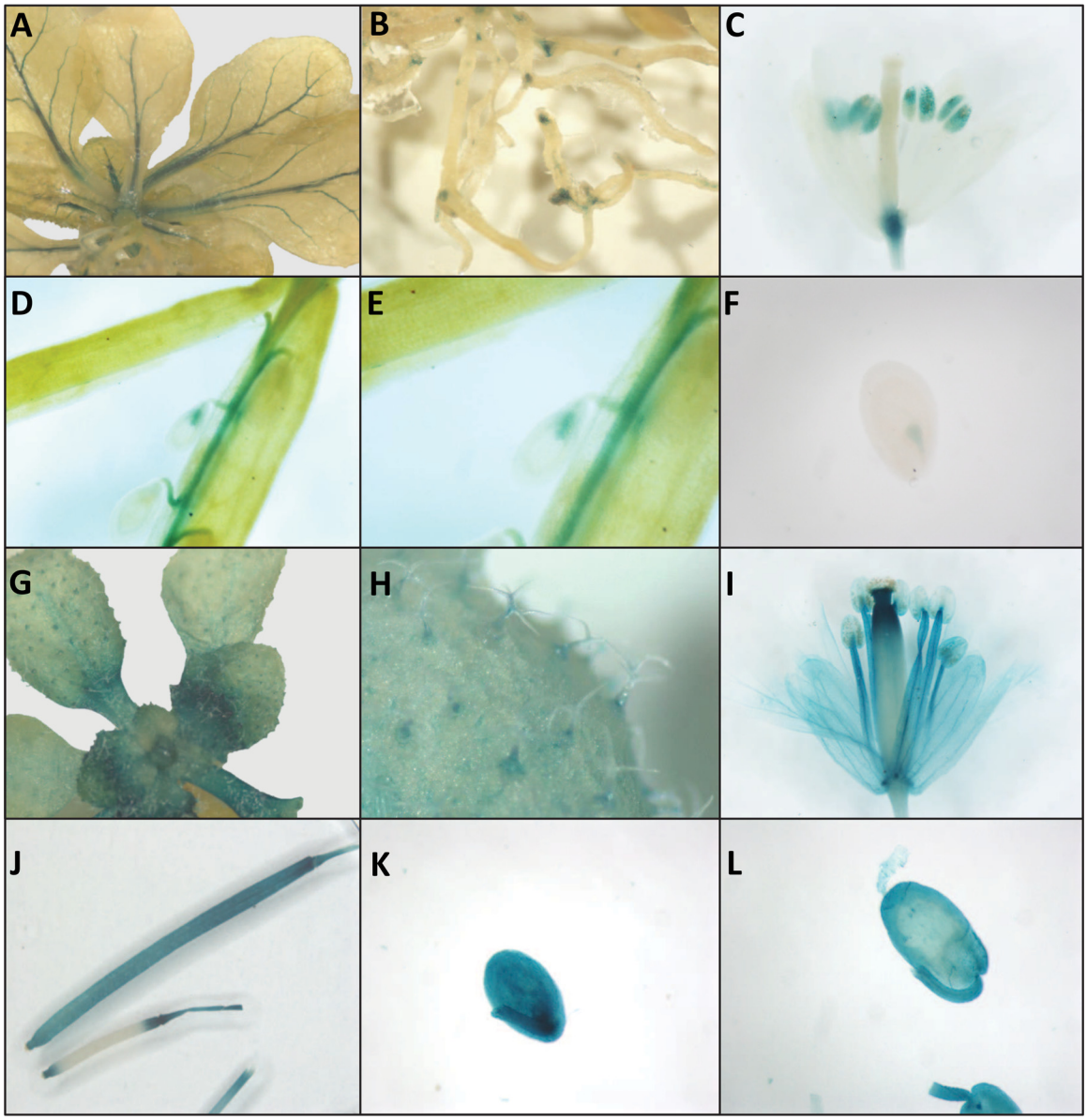

FIG. 5. **The promoter activity of *MLP28* and *MLP423* during Arabidopsis development.** *A*, GUS was active in the vascular tissue of rosette leaves of *MLP28*pro::GUS seedlings. *B*, In *MLP28*pro::GUS roots, *GUS* staining is restricted to lateral root meristems. *C*, In the reproductive tissues of *MLP28*pro::GUS plants, GUS activity is restricted to the pollen grains in anther pollen sacs and to the articulation on top of the pedicel. *D–F*, *GUS* staining was also observed in developing siliques and the embryonic tissues of developing seeds in *MLP28*pro::GUS plants. *G*, A low level of *GUS* activity was observed in all vegetative tissues of *MLP423*pro::GUS seedlings, but was at higher levels in the petioles and base of emerging or newly emerged leaves. *H*, *GUS* staining was concentrated at the base of rosette leaf trichomes in mature *MLP423*pro::GUS plants. *I*, In reproductive tissues, GUS activity was observed in sepals, petals and anther filaments as well as in the style of the pistil below the stigma in *MLP423*pro::GUS plants. *J*, In mature siliques, GUS was evenly active in *MLP423*pro::GUS plants, however, in maturing siliques of this transformant line *GUS* staining was restricted to terminal regions. *K–L*, *GUS* was evenly active through *MLP423pro*::GUS seeds.

shoot apex defects (Fig. 6*d-e*), occasioning premature death. Plants of a third transgenic line, amiR-MLP28 1.1, were wild-type in appearance and from RT-qPCR analysis had wild-type *MLP28* levels (Fig. 6*B* and 6*E*).

In addition to assessing *MLP28* expression in *mlp28* and the amiR-MLP28 lines, the transcript levels of *LCR*, *CLV3* and *WUS* were also analyzed. As expected, *LCR* expression remained at approximately wild-type levels in *mlp28* plants and in amiR-MLP28 1.1, 1.2 and 1.3 lines (Fig. 6*F*). The amiR-MLP28 1.2 and 1.3 lines had decreased *CLV3* expression (Fig. 6G), but surprisingly the repression was greater in amiR-MLP28 1.2 plants than in the 1.3 line (Fig. 6G), and the *WUS* levels were elevated to the greatest degree in *mlp28* and amiR-MLP28 1.1 plants, the two plant lines displaying wild-type like phenotypes and no change to *CLV3* expression (Fig. 6*A*–6*B* and 6*G*–6*H*). Together, the phenotypic

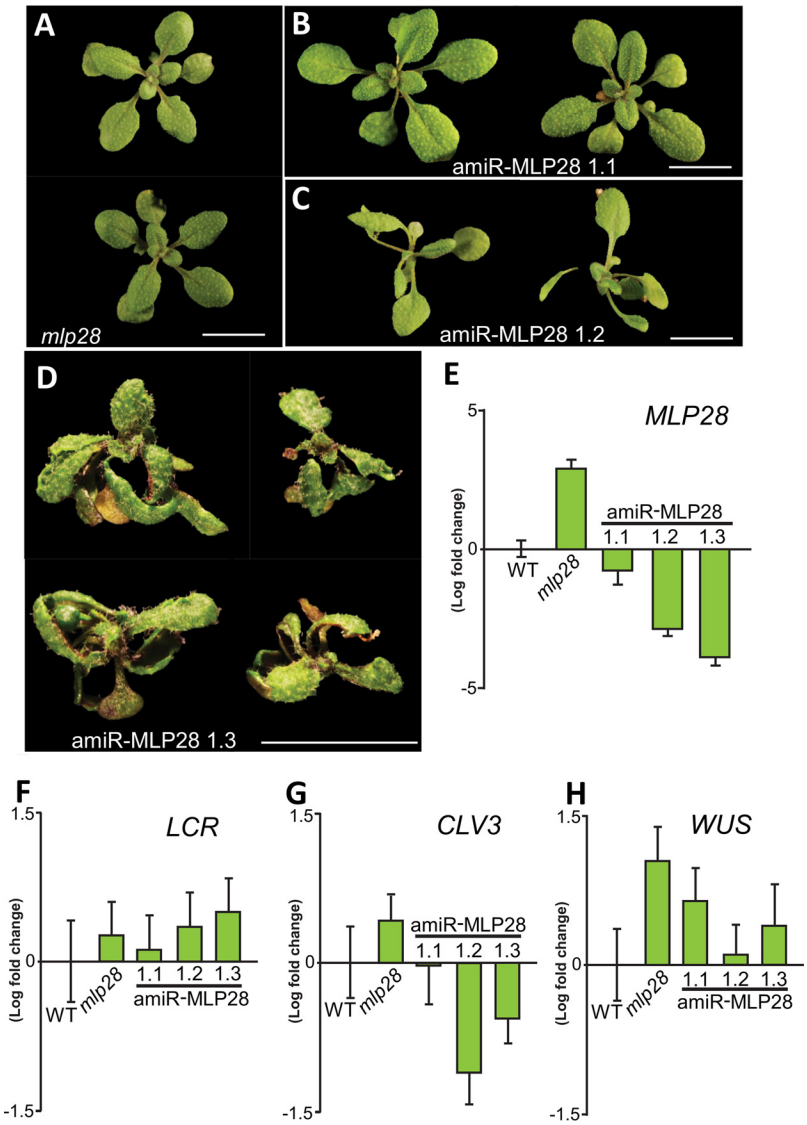

FIG. 6. **Analysis of Arabidopsis expressing the MLP28-targeting amiRNA, amiR-MLP28.** *A*, The *MLP28* T-DNA knockout insertion plant line *mlp28* (bottom of panel) is phenotypically indistinguishable from wild-type Arabidopsis (top of panel). *B*, Independent amiRNA transformant line amiR-MLP28 1.1 expressed a wild-type-like phenotype. *C*, The amiR-MLP28 1.2 transformants displayed mild developmental abnormalities, including elongated petioles and leaf curvature alterations. *D*, Transformant line amiR-MLP28 1.3 expressed the most severe developmental defects, including stunted growth and strong alterations in leaf patterning and morphology, and shoot apex defects. *E*, RT-qPCR analysis of *MLP28* expression in Arabidopsis shoot apex tissues transcripts. *F*, *LCR* expression in shoot apex tissues of Arabidopsis plants with altered *MLP28* levels. *G*, RT-qPCR analysis of *CLV3* expression in Arabidopsis shoot apex tissues. *H*, *WUS* expression was also assessed in Arabidopsis plant lines with altered *MLP28* levels via the RT-qPCR approach. *E–H*, *Cyclophilin* (*AT2G29960*) was used as normalization control and all expression analyses were repeated in triplicate on three biological replicates.

data suggest that reduced *MLP28* expression has severe consequences on Arabidopsis development, and furthermore, the molecular analyses indicate that *WUS* and *CLV3* are deregulated.

DISCUSSION

In plants, LCR F-box is highly conserved and is currently the only gene known to be targeted by miR394-directed post-transcriptional gene expression regulation (15, 13). The role of most functionally characterized F-box proteins is to target a specific protein or multiple proteins for ubiquitination and subsequent degradation via proteolysis in the 26S proteasome (1, 2). This suggests that the overall biological role of miR394 in Arabidopsis and other miR394 encoding plant species is to add an additional layer of regulation to the LCR F-box pathway.

Members of the F-box protein superfamily are characterized by a highly conserved 40–60 aa F-box motif in their N terminus (5, 45, 46). Structure predictions revealed that LCR F-box contains a conserved 47 aa F-box motif, and that this

motif is highly conserved across a diverse range of plant species (Table I and Fig. 1). Structural analysis also suggested that the F-box motif of LCR is likely to form a stem-like structure that protrudes from the body of LCR protein (Fig. 1*B*). Generally, the N-terminal F-box motif mediates F-box protein binding to SKP1 in the SCF complex (40, 47, 48, 8), and accordingly, the crystal structure of the previously characterized F-box TIR1 in association with ASK1, revealed an overall mushroom-shaped structure (49).

Previous protein-protein interaction studies have demonstrated that LCR F-box interacts with several ASK-like proteins, including ASK1 (40), and the structural predictions performed in this study (Fig. 1) strongly suggest that these protein-protein interactions are most likely mediated by the highly conserved F-box motif in the LCR N terminus. The LCR C terminus is predicted to form a β-propeller structure (Fig. 1*C*) and most likely confers the specificity of LCR F-box for its targeted protein(s), as previous research has demonstrated that the C-terminal region of individual F-box proteins encodes a variety of protein-binding domains that are usually responsible for substrate recognition by the SCF complex (5, 50, 51). However, the target proteins of most of the many hundreds of currently identified plant-specific F-box proteins remain to be experimentally determined.

Here, molecular approaches were taken to generate and study Arabidopsis lines with altered *LCR* expression. In LCR-OE line, a LCR-targeted protein would be expected to be rapidly degraded and therefore only accumulate to very low or even undetectable levels. Conversely, LCR-targeted proteins would be expected to have enhanced accumulation in Arabidopsis lines with reduced LCR levels, namely in LCR-KD plants. Comparative MS-based analysis identified members of two protein families, the MLP and SOUL protein families as putative candidates for LCR-mediated post-translational gene expression regulation, because of their differential accumulation in LCR-OE and LCR-KD plant lines (Fig. 3). SOUL proteins are ubiquitous in nature, functioning as tetrapyrrole carrier proteins in animals (52, 53). In plants, tetrapyrroles include compounds such as chlorophyll and heme; however, the functional role that SOUL proteins mediate in plant cells remains to be determined (54–56). Although SOUL was identified as a differentially expressed candidate protein by MS, subsequent molecular-based approaches to assess whether LCR directly post-translationally regulates SOUL protein stability were unsuccessful and therefore require further experimental investigation.

Members of the second group of MS-identified putative LCR target proteins, the MLP protein family, were first identified in opium poppy (*Papaver somniferum*) as latex-specific polypeptides (57), and have because been found to be highly conserved in plants (58, 59). Although the *Arabidopsis* MLP protein family consists of twenty-four members (58, 59), only peptides derived from family member MLP28 showed differential accumulation in LCR-OE and LCR-KD plants by LC-MS/MS. Additional analyses revealed that MLP family members are closely structurally related to one another (supplemental Fig. S3 and S4), and furthermore, that in addition to MLP28, *Arabidopsis* MLP family members MLP31, MLP34, MLP43, and MLP423 were also regulated but to differing degrees, by LCR F-box (Fig. 4). Together, the structural and molecular-based results reported here strongly indicated that MLP protein family members might be targeted by LCR F-box for post-translational gene expression regulation.

The structure of Arabidopsis MLP28 has previously been experimentally determined and demonstrated to be structurally related to members of the Bet v1 (from the *Betula verrucosa*) protein superfamily (58). Bet v1 proteins are characterized by the presence of hydrophobic pockets in their tertiary structure and compounds that are structurally similar to brassinosteroids and cytokinins have been shown to 'occupy' these hydrophobic pockets (60–63). Indeed, the predicted structure of all analyzed members of the *Arabidopsis* MLP protein family showed high modeling confidence and aa identity with the Bet v1 superfamily proteins, Cytokinin-Specific Binding Protein (CSBP) and Pyrabactin Resistance [PYR]/PYR-Llike 3 (PYL3). *CSBP* and *PYL3* encode a cytokinin binding protein and an abscisic acid (ABA) receptor respectively (63, 64), and together these analyses indicate that Arabidopsis MLP proteins could also potentially bind compounds with structural similarity to plant hormones in their hydrophobic pockets.

The post-transcriptional regulation of the TIR1 F-box by miR393 is well established (12, 65). TIR1 post-translationally targets several Aux/IAA family members for ubiquitin-mediated degradation (12, 65). Aux/IAAs are transcription regulators that repress the expression of several auxin-responsive genes and all 29 Aux/IAAs encoded by Arabidopsis are regulated to different degrees by TIR1 (66–68). TIR1 is a hormone receptor and a hydrophobic pocket on the upper surface of the C terminus of TIR1 presents a binding site for auxin to allow TIR1 to act as the 'molecular glue' for Aux/IAA target protein interaction (49). If LCR F-box targets *MLP* gene family members for ubiquitin-mediated degradation, a similar F-box/hormone-pocket/F-box-target mechanism can be envisaged for LCR F-box interaction with its MLP targets.

The detection of physical interaction between LCR and MLP423, and not between LCR and MLP28 was perplexing. The LC-MS/MS data clearly showed that of all the Arabidopsis *MLP* gene family members, only the accumulation of MLP28 was affected in the shoot apex tissue of LCR-OE and LCR-KD lines. In addition, Western blot analysis clearly demonstrated that LCR co-infiltration had a greater impact on MLP28 levels than on MLP423 accumulation. Together, these results indicate that LCR preferentially interacts with MLP28 over MLP423, but this preferential interaction could not be confirmed by the transient BiFC approach. One possible scenario is that LCR can interact with either MLP, but triggers ubiquitination of MLP28 at a much greater rate than its me-

diated ubiquitination of MLP423. This would lead to the rapid degradation of the N-terminal fused YFP version of MLP28, thus preventing the generation of visible fluorescent signals in LCR:cYFP/MLP28:nYFP co-expressing cells. Conversely, a slower rate of LCR-mediated ubiquitination of the less preferred target, MLP423, would allow *in planta* detection of physical LCR/MLP423 interaction and YFP visualization.

Although a physical interaction between MLP28 and LCR F-box was not detected, our promoter::GUS transgene results showed that the expression patterns of *MLP28*, *MLP423*, *LCR* and *LCR*-targeting miRNA, *MIR394*, overlap in specific Arabidopsis tissues and stages of development (Fig. 5 and supplemental Fig. S5). The vascular-restricted expression of *MLP28* is consistent with the expression profile of latex-specific *MLP* genes in opium poppy (57). Additionally, MLP328 and MLP329 have been detected in Arabidopsis phloem sap, leading to the suggestion that they are involved in long-distance signaling and lipid transport (69). Interestingly, our analyses revealed that *MIR394A* is also expressed in the vascular tissue of young rosette leaves (supplemental Fig. S5), and aberrant vascular pattern formation has been described in an Arabidopsis plant transformed with a miR394-resistant *LCR* transgene (13). The promoter::GUS transgene approach also clearly demonstrated that all assessed loci, including *MLP28*, *MLP423*, *LCR*, *MIR394A,* and *MIR394B*, has their promoter active in the shoot apices, and the tissues surrounding this region, including the petioles and bases of emerging, or newly emerged leaves (Fig. 5 and supplemental Fig. S5). These expression data not only support previous microarray-based expression data for each of the analyzed loci (70), but further suggest that the miR394/LCR/MLP relationship forms a crucial gene expression regulation module in tissues that are central to Arabidopsis development.

The major developmental defects observed in Arabidopsis plants, when miR394-directed post-transcriptional repression of *LCR* is lost, are concentrated in the shoot apex region during the early stages of vegetative development. The leaves of LCR-OE plants are strongly downwardly curled and, in severe phenotypes, meristem aberration impairs further plant development (Fig. 2 and supplemental Fig. S2). If the developmental defects displayed by LCR-OE plants were the result of enhanced LCR F-box-mediated post-translational gene expression regulation of MLP28, then plants with reduced *MLP28* levels would be expected to express similar developmental phenotypes. Plants of two independent transgenic lines, expressing amiRNAs that reduce the expression of *MLP28*, displayed a range of phenotype abnormalities, from mild changes in leaf curvature through to the development of tiny plants with dramatic changes in leaf patterning and morphology and shoot apex defects (Fig. 6*C* and 6*D*). These phenotypes that are highly suggestive of deficiencies in SAM development and resemble those displayed by Arabidopsis plants in which *LCR* expression is no longer correctly regulated by miR394 (Fig. 2 and supplemental Fig. S2). The target protein(s) of LCR F-box has previously been suggested to enable the correct coordination of stem cell fate in the SAM, and that this is orchestrated by LCR F-box target protein(s) mediating the expression of SAM regulators, *WUS* and *CLV3* (16). Indeed, slight perturbations in *CLV3*/*WUS* gene expression is presented herein, where *CLV3* levels were altered in both LCR-OE and amiR-MLP28 lines that displayed developmental abnormalities. Curiously, a corresponding increase in *WUS* expression in these lines was not detectable although this may be because of difficulties in measuring genes that are expressed in only a few cells within the SAM.

Here we show that the miR394-regulated F-Box LCR degrades MLP proteins, and provides extensive evidences to suggest that *MLP* gene family, specifically *MLP28* and *MLP423*, are target of miR394-LCR regulatory node, representing potential targets for post-translational gene expression regulation by LCR. In addition, and that is critical for normal Arabidopsis development. We propose that MLP28 and MLP423 family members are associated with the LCR regulation and a miR394/LCR/MLP regulatory module might exist in the shoot apical meristem, being critical for normal plant development.

Acknowledgments—We thank Dr. Deborah Barton (University of Sydney) for the confocal microscopy. Also thanks to Dr. Julia Bally (Queensland University of Technology) and Dr. Harsh Garg (University of Sydney) for technical support, and Prof. Fabio T.S. Nogueira (University of São Paulo) for his encouragement.

* CGLJ was the recipient of a CAPES Foundation Scholarship, Ministry of Education of Brazil (Process BEX no. 040509-4).

S This article contains supplemental materials.

§§ To whom correspondence should be addressed: The University of Sydney, School of Biological Sciences, University of Sydney, Camperdown NSW, Sydney 2006. Australia. Tel.: Phone: +61 (7) 31387793; E-mail: cgli2101@uni.sydney.edu.au.

The authors declare that they have no competing interests.

REFERENCES

1. DeMartino, G. N., and Gillette, T. G. (2007) Proteasomes: machines for all reasons. *Cell* **129,** 659–362
2. Weissman, A. M., Shabek, N., and Ciechanover, A. (2011) The predator becomes the prey: regulating the ubiquitin system by ubiquitylation and degradation. *Nat. Rev. Mol. Cell Biol.* **12,** 605–620
3. Kleiger, G., Mayor, T. (2014) Perilous journey: a tour of the ubiquitin–proteasome system. *Trends Cell Biol.* **24,** 352–359
4. Vierstra, R. D. (2009) The ubiquitin-26S proteasome system at the nexus of plant biology. *Nat. Rev. Mol. Cell Biol.* **10,** 385–397
5. Gagne, J. M., Downes, B. P., Shiu, S. H., Durski, A. M., and Vierstra, R. D. (2002) The F-box subunit of the SCF E3 complex is encoded by a diverse superfamily of genes in Arabidopsis. *Proc. Natl. Acad. Sci. U.S.A.* **99,** 11519–11524
6. Xu G., Ma, H., Nei, M., and Kong, H. (2009) Evolution of F-box genes in plants: different modes of sequence divergence and their relationships with functional diversification. *Proc. Natl. Acad. Sci. U.S.A.* **106,** 835–840
7. Deshaies, R. J., and Joazeiro, C. A. P. (2009) RING domain E3 ubiquitin ligases. *Annu. Rev. Biochem.* **78,** 399–434
8. Skaar, J. R., Pagan, J. K., and Pagano, M. (2013) Mechanisms and function of substrate recruitment by F-box proteins. *Nat. Rev. Mol. Cell Biol.* **14,** 369–381
9. Zheng, N., Schulman, B. A., Song, L., Miller, J. J., Jeffrey, P. D., Wang, P. Chu, C., Koepp, D. M., Elledge, S. J., Pagano, M., Conaway, R. C., Conaway, J. W., Harper, J. W., and Pavletich, N. P. (2002) Structure of

the Cul1-Rbx1-Skp1-F boxSkp2 SCF ubiquitin ligase complex. *Nature* **416,** 703–709
10. Somers, D. E., and Fujiwara, S. (2009) Thinking outside the F-box: novel ligands for novel receptors. *Trends Plant Sci.* **14,** 206–213
11. Lechner, E., Achard, P., Vansiri, A., Potuschak, T., and Genschik, P. (2006) F-box proteins everywhere. *Curr. Opin. Plant Biol.* **9,** 631–638
12. Parry, G., Calderon-Villalobos, L. I., Prigge, M., Peret, B., Dharmasiri, S., Itoh, H., Lechner, E., Gray, W. M., Bennett, M., and Estelle, M. (2009) Complex regulation of the TIR1/AFB family of auxin receptors. *Proc. Natl. Acad. Sci. U.S.A.* **106,** 22540–22545
13. Song, J. B., Huang, S. Q., Dalmay, T., and Yang, Z. M. (2012) Regulation of leaf morphology by microRNA394 and its target leaf curling responsiveness. *Plant Cell Physiol.* **53,** 1283–1294
14. Lima, J. C., Arenhart, R. A., Margis-Pinheiro, M., and Margis, R. (2011) Aluminium triggers broad changes in microRNA expression in rice roots. *Genet. Mol. Res.* **10,** 2817–2832
15. Jones-Rhoades, M. W., and Bartel, D. P. (2004) Computational identification of plant microRNAs and their targets, including a stress-induced miRNA. *Mol. Cell* **14,** 787–799
16. Knauer, S., Holt, A. L., Rubio-Somoza, I., Tucker, E. J., Hinze, A., Pisch, M., Javelle, M., Timmermans, M. C., Tucker, M. R., and Laux, T. (2013) A protodermal miR394 signal defines a region of stem cell competence in the Arabidopsis shoot meristem. *Dev. Cell* **24,** 125–132
17. Song, J., Gao, S., Sun, D., Li, H., Shu, X., and Yang, Z. (2013) miR394 and LCR are involved in Arabidopsis salt and drought stress responses in an abscisic acid-dependent manner. *BMC Plant Biol.* **13,** 210–226
18. Alonso, J. M., Stepanova, A. N., Leisse, T. J., Kim, C. J., Chen, H., Shinn, P., Stevenson, D. K., Zimmerman, J., Barajas, P., Cheuk, R., Gadrinab, C., Heller, C., Jeske, A., Koesema, E., Meyers, C. C., Parker, H., Prednis, L., Ansari, Y., Choy, N., Deen, H., Geralt, M., Hazari, N., Hom, E., Karnes, M., Mulholland, C., Ndubaku, R., Schmidt, I., Guzman, P., Aguilar-Henonin, L., Schmid, M., Weigel, D., Carter, D. E., Marchand, T., Risseeuw, E., Brogden, D., Zeko, A., Crosby, W. L., Berry, C. C., and Ecker, J. R. (2003) Genome-wide insertional mutagenesis of Arabidopsis thaliana. *Science* **301,** 653–657
19. Zhang, X., Henriques, R., Lin, S. S., Niu, Q. W., and Chua, N. H. (2006) Agrobacterium-mediated transformation of Arabidopsis thaliana using the floral dip method. *Nat. Protoc.* **1,** 641–646
20. Ruiz, M. T., Voinnet, O., and Baulcombe, D. C. (1998) Initiation and maintenance of virus-induced gene silencing. *Plant Cell* **10,** 937–946
21. Gleave, A. (1992) A versatile binary vector system with a T-DNA organisational structure conducive to efficient integration of cloned DNA into the plant genome. *Plant Mol. Biol.* **20,** 1203–1207
22. Stintzi, A., and Browse, J. (2000) The Arabidopsis male-sterile mutant, opr3, lacks the 12-oxophytodienoic acid reductase required for jasmonate synthesis. *Proc. Natl. Acad. Sci. U.S.A.* **97,** 10625–10630
23. Earley, K. W., Haag, J. R., Pontes, O., Opper, K., Juehne, T., Song, K., and Pikaard, C. S. (2006) Gateway-compatible vectors for plant functional genomics and proteomics. *Plant J.* **45,** 616–629
24. Chakrabarty, R., Banerjee, R., Chung, S-M., Farman, M., Citovsky, V., Hogenhout, S. A., Tzfira, T., and Goodin, M. (2007) pSITE vectors for stable integration or transient expression of autofluorescent protein fusions in plants: probing Nicotiana benthamiana-virus interactions. *Mol. Plant-Microbe Interact.* **20,** 740–750
25. Martin, K., Kopperud, K., Chakrabarty, R., Banerjee, R., Brooks, R., and Goodin, M. M. (2009) Transient expression in Nicotiana benthamiana fluorescent marker lines provides enhanced definition of protein localization, movement and interactions in planta. *Plant J.* **59,** 150–162
26. Fang, Y., and Spector, D. L. (2010) BiFC imaging assay for plant protein-protein interactions. *Cold Spring Harbor Protocols* **2010** (2), pdb. prot5380
27. Johnson, C. S., Kolevski, B., and Smyth, D. R. (2002) Transparent testa glabra2, a trichome and seed coat development gene of Arabidopsis, encodes a WRKY transcription factor. *Plant Cell* **14,** 1359–1375
28. Eamens, A., and Waterhouse, P. (2011) Vectors and methods for hairpin RNA and artificial microRNA-mediated gene silencing in plants. *Methods Mol. Biol.* **701,** 179–197
29. Gammulla, C. G., Pascovici, D., Atwell, B. J., and Haynes, P. A. (2011) Differential proteomic response of rice (Oryza sativa) leaves exposed to high- and low-temperature stress. *Proteomics* **11,** 2839–2850
30. Parker, B. L., Larsen, M. R., Edvinsson, L. I. H., and Povlsen, G. K. (2013) Signal transduction in cerebral arteries after subarachnoid hemorrhage—a phosphoproteomic approach. *J. Cereb. Blood Flow Metab.* **33,** 1259–1269
31. Boersema, P. J., Raijmakers, R., Lemeer, S., Mohammed, S., and Heck, A. J. R. (2009) Multiplex peptide stable isotope dimethyl labeling for quantitative proteomics. *Nat. Protoc.* **4,** 484–494
32. Käll, L., Canterbury, J. D., Weston, J., Noble, W. S., and MacCoss, M. J. (2007) Semi-supervised learning for peptide identification from shotgun proteomics datasets. *Nat. Methods* **4** (11), 923–925
33. Vizcaíno, J. A., Deutsch, E. W., Wang, R., Csordas, A., Reisinger, F., Ríos, D., Dianes, J. A., Sun, Z., Farrah, T., Bandeira, N., Binz, P. A., Xenarios, I., Eisenacher, M., Mayer, G., Gatto, L., Campos, A., Chalkley, R. J., Kraus, H. J., Albar, J. P., Martinez-Bartolomé, S., Apweiler, R., Omenn, G. S., Martens, L., Jones, A. R., and Hermjakob, H. (2014) ProteomeXchange provides globally coordinated proteomics data submission and dissemination. *Nat. biotechnol.* **32** (3), 223–226
34. Altschul, S. F., Gish, W., Miller, W., Myers, E. W., and Lipman, D. J. (1990) Basic local alignment search tool. *J. Mol. Biol.* **215,** 403–410
35. Punta, M., Coggill, P. C., Eberhardt, R. Y., Mistry, J., Tate, J., Boursnell, C., Pang, N., Forslund, K., Ceric, G., Clements, J., Heger, A., Holm, L., Sonnhammer, E. L. L., Eddy, S. R., Bateman, A., and Finn, R. D. (2012) The Pfam protein families database. *Nucleic Acids Res.* **40** (D1), D290–D301
36. Andrade, M. A., Ponting, C. P., Gibson, T. J., and Bork, P. (2000) Homology-based method for identification of protein repeats using statistical significance estimates. *J. Mol. Biol.* **298,** 521–537
37. Kelley, L. A., and Sternberg, M. J. E. (2009) Protein structure prediction on the web: a case study using the Phyre server. *Nat. Protoc.* (3), 363–371
38. Ramachandran, S., Kota, P., Ding, F., and Dokholyan, N. V. (2011) Automated minimization of steric clashes in protein structures. *Proteins: Struct., Funct., Bioinf.* **79,** 261–270
39. Szklarczyk, D., Franceschini, A., Kuhn, M., Simonovic, M., Roth, A., Minguez, P., Doerks, T., Stark, M., Muller, J., Bork, P., Jensen, L. J., and von Mering C. (2011) The STRING database in 2011: functional interaction networks of proteins, globally integrated and scored. *Nucleic Acids Res.* **39** (suppl 1), D561–D568
40. Risseeuw, E. P., Daskalchuk, T. E., Banks, T. W., Liu, E., Cotelesage, J., Hellmann, H., Estelle, M., Somers, D. E., and Crosby, W. L. (2003) Protein interaction analysis of SCF ubiquitin E3 ligase subunits from Arabidopsis. *Plant J.* **34,** 753–767
41. Ebert, M. S., Neilson, J. R., and Sharp, P. A. (2007) MicroRNA sponges: competitive inhibitors of small RNAs in mammalian cells. *Nat. Methods* **4,** 721–726
42. Yan, J., Gu, Y., Jia, X., Kang, W., Pan, S., Tang, X., Chen, X., and Tang, G. (2012) Effective Small RNA Destruction by the Expression of a Short Tandem Target Mimic in Arabidopsis. *Plant Cell* **24,** 415–427
43. Schwab, R., Ossowski, S., Riester, M., Warthmann, N., and Weigel, D. (2006) Highly specific gene silencing by artificial microRNAs in Arabidopsis. *Plant Cell* **18,** 1121–1133
44. Eamens, A., McHale, M., and Waterhouse, P. (2014) The use of artificial microRNA technology to control gene expression in Arabidopsis thaliana. *Methods Mol. Biol.* **1062,** 211–224
45. Xiao, W., and Jang, J-C. (2000) F-box proteins in Arabidopsis. *Trends Plant Sci.* **5,** 454–457
46. Kipreos, E. T., and Pagano, M. (2000) The F-Box protein family. *Genome Biol.* **1**, R3002.1-R3002.7
47. Farras, R., Ferrando, A., Jasik, J., Kleinow, T., Okresz, L., Tiburcio, A., Salchert, K., del Pozo, C., Schell, J., and Koncz C. (2001) SKP1-SnRK protein kinase interactions mediate proteasomal binding of a plant SCF ubiquitin ligase. *EMBO J.* **20,** 2742–2756
48. Durfee, T., Roe, J. L., Sessions, R. A., Inouye, C., Serikawa, K., Feldmann, K. A., Weigel, D., and Zambryski, P. C. (2003) The F-box-containing protein UFO and AGAMOUS participate in antagonistic pathways governing early petal development in Arabidopsis. *Proc. Natl. Acad. Sci. U.S.A.* **100,** 8571–8576
49. Tan, X., Calderon-Villalobos, L. I. A., Sharon, M., Zheng, C., Robinson, C. V., Estelle, M., and Zheng, N. (2007) Mechanism of auxin perception by the TIR1 ubiquitin ligase. *Nature* **446,** 640–645
50. Adams, J., Kelso, R., and Cooley, L. (2000) The kelch repeat superfamily of proteins: propellers of cell function. *Trends Cell Biol.* **10,** 17–24
51. Andrade, M., González-Guzmán, M., Serrano, R., and Rodríguez, P. A.

(2001) Combination of the F-box motif and Kelch repeats defines a large Arabidopsis family of F-box proteins. *Plant Mol. Biol.* **46,** 603–614
52. Blackmon, B. J., Dailey T. A., Lianchun, X., and Dailey, H. A. (2002) Characterization of a human and mouse tetrapyrrole-binding protein. *Arch. Biochem. Biophys.* **407,** 196–201
53. Babusiak, M., Man, P., Sutak, R., Petrak, J., and Vyoral, D. (2005) Identification of heme binding protein complexes in murine erythroleukemic cells: Study by a novel two-dimensional native separation–liquid chromatography and electrophoresis. *Proteomics* **5,** 340–350
54. Takahashi, S., Ogawa, T., Inoue, K., and Masuda, T. (2008) Characterization of cytosolic tetrapyrrole-binding proteins in Arabidopsis thaliana. *Photochem. Photobiol. Sci.* **7,** 1216–1224
55. Dias, J. S., Macedo, A. L., Ferreira, G. C., Peterson, F. C., Volkman, B. F., and Goodfellow, B. J. (2006) The first structure from the SOUL/HBP family of heme-binding proteins, Murine P22HBP. *J. Biol. Chem.* **281,** 31553–31561
56. Lee, H-J., Mochizuki, N., Masuda, T., and Buckhout, T. J. (2012) Disrupting the bimolecular binding of the haem-binding protein 5 (AtHBP5) to haem oxygenase 1 (HY1) leads to oxidative stress in Arabidopsis. *J. Exp. Bot.* **63,** 5967–5978
57. Nessler, C. L., Allen, R. D., and Galewsky, S. (1985) Identification and characterization of latex-specific proteins in opium poppy. *Plant Physiol.* **79,** 499–504
58. Lytle, B. L., Song, J., de la Cruz, N. B., Peterson, F. C., Johnson, K. A., Bingman, C. A., Phillips Jr., G. N., and Volkman, B. F. (2009) Structures of two Arabidopsis thaliana major latex proteins represent novel helix-grip folds. *Proteins: Struct. Funct. Bioinf.* **76,** 237–243
59. Guo, D., Wong, W., Xu, W., Sun, F., Qing, D., and Li, N. (2011) Cis-cinnamic acid-enhanced 1 gene plays a role in regulation of Arabidopsis bolting. *Plant Mol. Biol.* **75,** 481–495
60. Iyer, L. M., Koonin, E. V., and Aravind, L. (2001) Adaptations of the helix-grip fold for ligand binding and catalysis in the START domain superfamily. *Proteins: Struct. Funct. Bioinf.* **43,** 134–144
61. Tsujishita, Y., and Hurley, J. H. (2000) Structure and lipid transport mechanism of a StAR-related domain. *Nat. Struct. Mol. Biol.* **7,** 408–414
62. Marković-Housley, Z., Degano, M., Lamba, D., von Roepenack-Lahaye, E., Clemens, S., Susani, M., Ferreira, F., Scheiner, O., Breiteneder, H. (2003) Crystal structure of a hypoallergenic isoform of the Major Birch Pollen Allergen Bet v 1 and its likely biological function as a plant steroid carrier. *J. Mol. Biol.* **325,** 123–133
63. Pasternak, O., Bujacz, G. D., Fujimoto, Y., Hashimoto, Y., Jelen, F., Otlewski, J., Sikorskia, M. M., and Jaskolski, M. (2006) Crystal structure of Vigna radiata cytokinin-specific binding protein in complex with zeatin. *Plant Cell* **18,** 2622–2634
64. Zhang, X., Zhang, Q., Xin, Q., Yu, L., Wang, Z., Wu, W., Jiang, L., Wang, G., Tian, W., Deng, Z., Wang, Y., Liu, Z., Long, J., Gong, Z., and Chen, Z. (2012) Complex structures of the abscisic acid receptor PYL3/RCAR13 reveal a unique regulatory mechanism. *Structure* **20,** 780–790
65. Si-Ammour, A., Windels, D., Arn-Bouldoires, E., Kutter, C., Ailhas, J., Meins Jr., F., and Vazquez, F. (2011) miR393 and secondary siRNAs regulate expression of the TIR1/AFB2 auxin receptor clade and auxin-related development of Arabidopsis leaves. *Plant Physiol.* **157,** 683–691
66. Dreher, K. A., Brown, J., Saw, R. E., and Callis, J. (2006) The Arabidopsis Aux/IAA protein family has diversified in degradation and auxin responsiveness. *Plant Cell* **18,** 699–714
67. dos Santos Maraschin, F., Memelink, J., and Offringa, R. (2009) Auxin-induced, SCFTIR1-mediated poly-ubiquitination marks AUX/IAA proteins for degradation. *Plant J.* **59,** 100–109
68. Calderón-Villalobos, L. I. A., Lee, S., de Oliveira, C., Ivetac, A., Brandt, W., Armitage, L., Sheard, L. B., Tan, X., Parry, G., Mao, H., Zheng, N., Napier, R., Kepinski, S., and Estelle, M. (2012) A combinatorial TIR1/AFB–Aux/IAA co-receptor system for differential sensing of auxin. *Nat. Chem. Biol.* **8,** 477–485
69. Guelette, B. S., Benning, U. F., and Hoffmann-Benning, S. (2012) Identification of lipids and lipid-binding proteins in phloem exudates from Arabidopsis thaliana. *J. Exp. Bot.* **63,** 3603–3616
70. Winter, D., Vinegar, B., Nahal, H., Ammar, R., Wilson, G. V., and Provart, N. J. (2007) An "Electronic Fluorescent Pictograph" browser for exploring and analyzing large-scale biological data sets. *PLoS ONE* **2,** e718